CHAPTER IV
RESULTS AND DISCUSSIONS

4.1 Design and developed of molecular sensors for saccharides

Our research has focused on the design and synthesis of molecular sensors for detection of saccharides in aqueous systems. Normally, molecular sensors consist of binding units and sensory units connecting with the linker. According to supramolecular chemistry, recognition incidence occurs through covalent bond and non-covalent interaction including hydrogen bound, ion-dipole interaction, electroststic interactions, π-π stacking interaction and cation-π interactions. [1] Therefore, the interaction between two substances showed significant role in biological process due to the specificity and sensitivity. It is well known that boronic acid is an excellent receptor unit for binding selectively with saccharides.

The most common used boronic acids as good receptors for binding selectively with saccharides rely on the reversible formation of cyclic ester with diols of sugar molecules. The boronic acid-saccharide interacts with 1,2- and 1,3- diols of saccharides to form five- or six- membered rings via covalent bonds, high stability and low toxicity [92]. Boronic acid group is an electron-deficient Lewis acid having a sp^2-hybridized boron atom with a trigonal conformation and electron rich having a sp^3-hybridized boron atom with a tetrahedral geometry, which is dependent on saccharide in system. Therefore, we designed 3-aminophenylboronic acid moieties for binding sugar. [93-94] Moreover, 1,8-naphthalamide and coumarin are anticipated to be the best fluorophone because naphthalamide and coumarin offered a highly fluorescence and photostable molecule [89,95].

Thus, in this work, we synthesized fluorescent sensor containing boronic acid as a binding site for saccharides upon the different fluorophores including coumarin and naphtalimide. For coumarin sensor, we have investigated the detection of saccharide by the interaction of boronic acid and diol-based saccharide. For another fluorescence sensor of naphtalimide, we employed gold nanoparticle regarding to the signaling amplifier in the sensing purpose. In both systems, the complexation studies were carried out by UV-Vis and fluorescence techniques.

4.2 The sensing studies of saccharide by Cum_B

4.2.1 Synthesis of Cum_B

The fluorescence sensor in this study contains 3- aminophenylboronic acid as a binding site and coumarin which performs a high emission band and photostable. The synthesis pathway of sensor **Cum_B** was illustrated in Scheme 4.1.

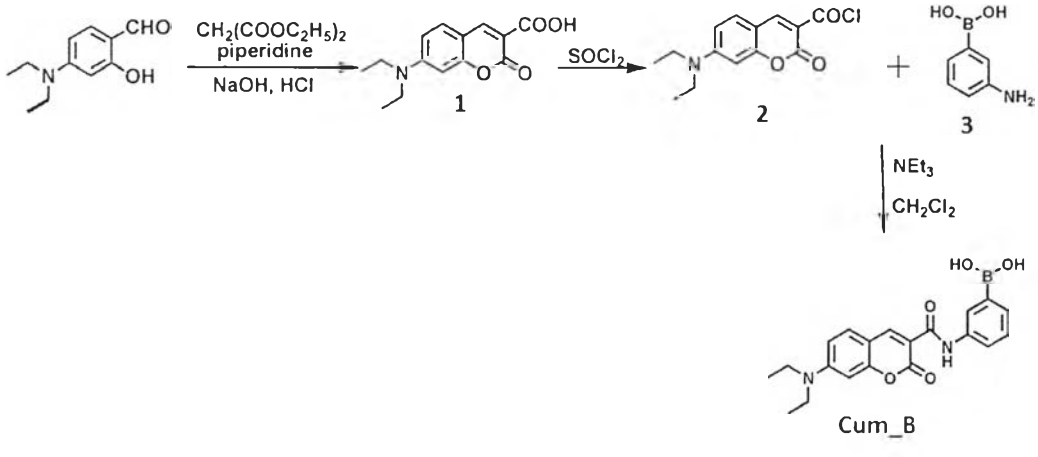

Scheme 4.1 Synthesis pathway of sensor **Cum_B**

Compound **1** was prepared by nucleophilic substitution of 4-diethylaminosalicyladehyde and diethylmalonate in ethanol under reflux conditions for 6 hours and purified by recrystallization to obtain an orange powder with 65%

yield. The ^{1}H-NMR spectrum showed the singlet of the carboxylic proton at 12.35 ppm and a singlet peak of the additional aromatic proton (C=CH-C) at 8.65 ppm. Then, the acid chloride compound **2** was synthesized by nucleophilic substitution between compound **1** and thionyl chloride upon stirring room temperature for 3 hours. The solution of compound **3** in dichlomethane was added directly into the conresponding compound **2** without the purification. The reaction was stirred at room temperature and the precipitate was collected and washed with dichlomethane to give yellow powder of **Cum_B** in 76% yield. The ^{1}H-NMR data of **Cum_B** displayed the disappearance of carboxylic proton at 12.35 ppm belonging to compound **1**. Interestingly, the singlet peak of proton of amide at 10.73 ppm and the additional aromatic protons of broronic acid at 8.09-7.71 ppm were observed in figure 4.1.

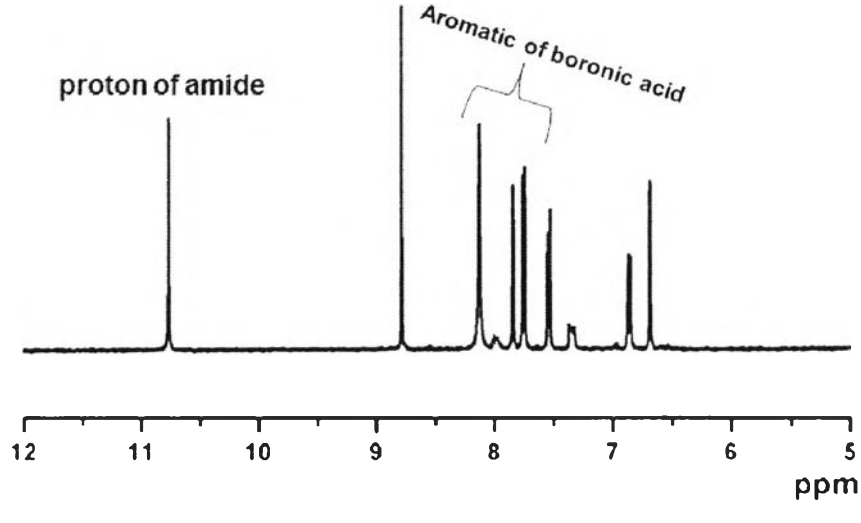

Figure 4.1 The ^{1}H-NMR spectrum of **Cum_B** in DMSO-d_6 (400 MHz).

4.3 Complexation studies

4.3.1 Complexation studies of sensor Cum_B with various saccharides

Sensor **Cum_B** also contains the boronic acid as a binding unit to covalently bind with saccharides and coumarin as a fluorophore. The sensor **Cum_B** was expected to form the covalent bond with hydroxyl group of saccharides. The absorption band and emission band of **Cum_B** in 5% DMSO with 0.1 M phosphate buffer at pH 7.4 were observed at 420 nm and 480 nm, respectively. The binding affinities of **Cum_B** in the presence of excess saccharides such as fructose, glucose, ribose, lactose, maltose and galactose were investigated by fluorescence spectrophotometry. Figure 4.2 presented the fluorescence of **Cum_B** with excess saccharides. The fluorescence intensity at 480 nm of **Cum_B** with guests was quenched, especially, fructose. The diol of saccharide could form the complex with boronic acid, inducing the sp^3 boron center of boronic acid. Consequently, the fluorescent quenching of the complexed **Cum_B** under photo-induced electron transfer (PET) process (scheme 4.2) was performed. Fluorescence quenching upon saccharides binding occurred by the electron transfer from phenyl group to coumarin. As a result, the switch-off fluorescence showed a promising selectivity for fructose over other saccharides. Actually, saccharide with five membered ring is preferred to bind covalently with boronic acid [96-100].

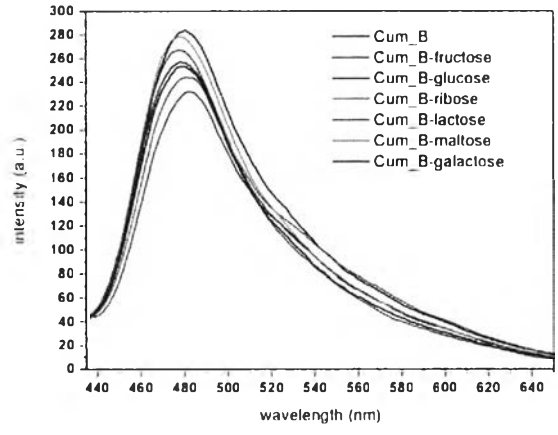

Figure 4.2 Fluorescence spectral changes of **Cum_B** with different sugars in 5 % DMSO with 0.1 M phosphate buffer at pH 7.4

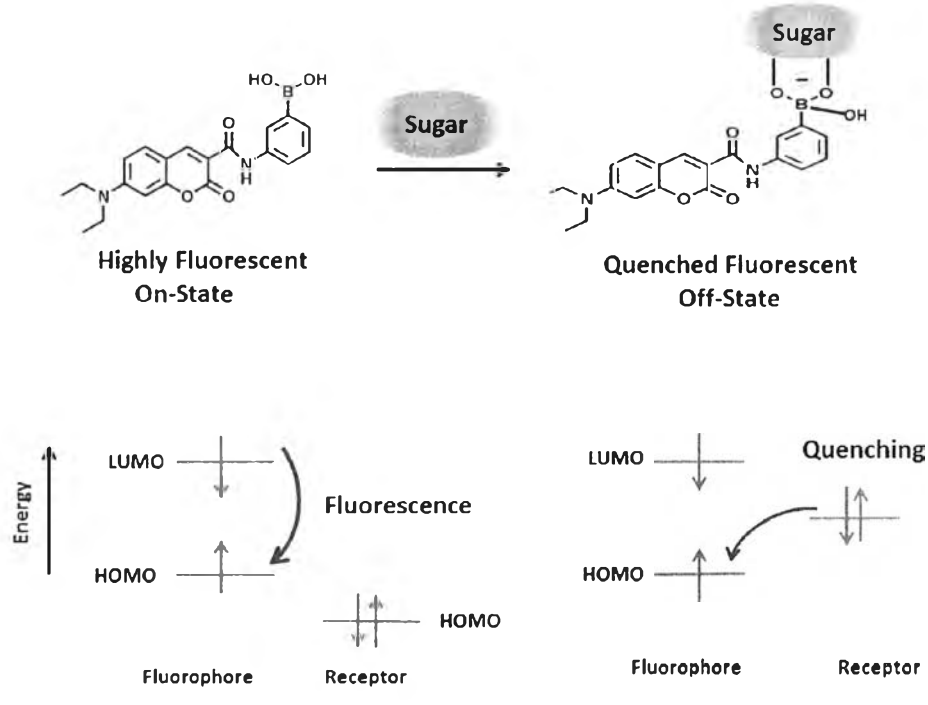

Scheme 4.2 Photoelectrochemical model used to illustrate PET fluorescence quenching and interaction between saccharide and **Cum_B** [95].

4.3.2 Complexation studies of sensor Cum_B with saccharides by fluorescence spectrophotometric titration technique

The fluorometric titration of sensor **Cum_B** with various saccharides was carried out in 5% DMSO with 0.1 M phosphate buffer at pH 7.4. Prior to fluorescence measurement, the solution mixture of the sensor and different saccharides was stirred for 30 minutes. From the fluorescence titration curve as diaplayed in figure 4.3, the emission band of **Cum_B** at 480 nm showed a decrease of the different ratio of intensity (I/I_0) at 480 nm upon the increment of guest. The change ratio (I/I_0) of **Cum_B** for fructose is higher than that of **Cum_B** for other saccharides. Moreover, the binding constant of sensor **Cum_B** toward fructose in 5% DMSO with phosphate buffer at pH 7.4 was approximately 5424 while the binding constants of **Cum_B** with other saccharides could not be determined because the fluorescence changes were not proportional to the concentration of guest (in Table 4.1). This suggested that fructose prefered to form a stable five-membered ring and a simple cyclic diols to the cis-comformation [96-100].

Table 4.1 Binding constant of sensor **Cum_B** with different saccharides.

Saccharides	K
Fructose	5424
Ribose	nd[a]
Galactose	nd[a]
Glucose	nd[a]
Lactose	nd[a]

a = not determined

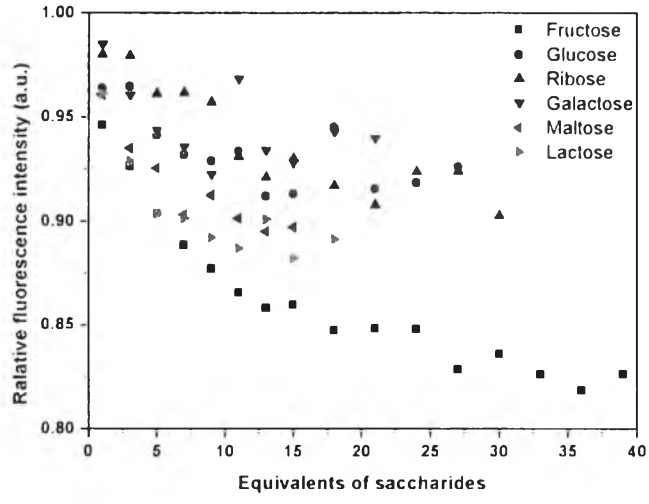

Figure 4.3 Relative fluorescence intensity ratios at 480 nm (I/Io) of **Cum_B** ($1x10^{-5}$ M) in the presence of 0-40 equiv. of difference saccharides in 5% DMSO: 0.1 M phosphate buffer pH 7.4.

The fluorescence titration was performed twices and the binding constant of **Cum_B** with fructose (fig 4.4) calculated by using Benesi-Hidebrand plot (fig 4.4 (b)) and equation 4.1. [68]

$$\frac{I_o}{I-I_0} = \frac{\alpha}{K_s[\mathrm{M}]} + \alpha \qquad 4.1$$

Where I_o is initial intensity; I is intensity of a particular concentration of guest; α is point of intersection of Y axis; K_s is binding constant of the sensor with the guest and [M] is the concentration of guest [68].

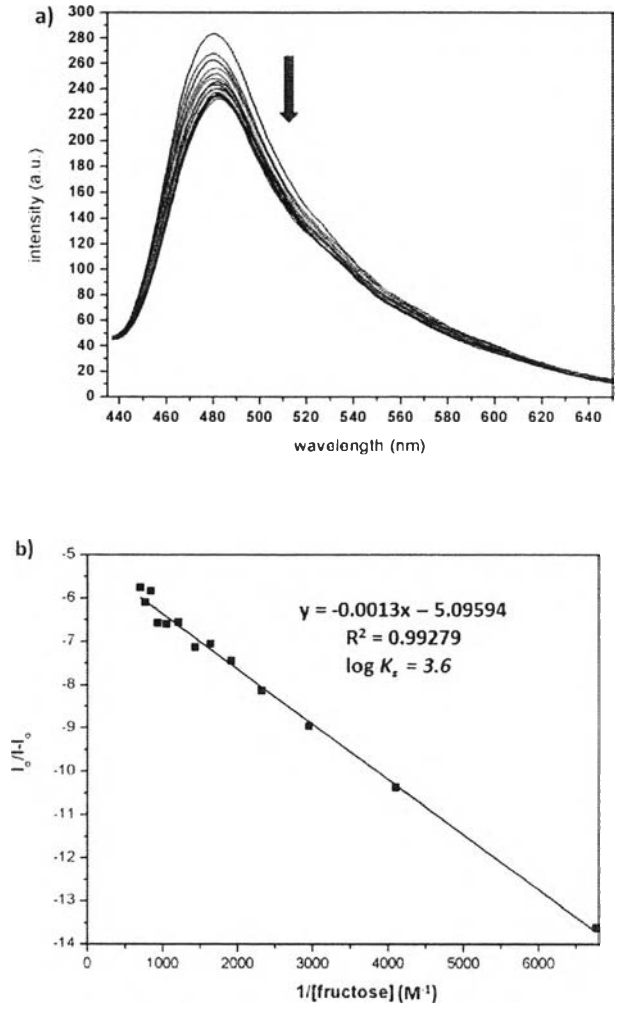

Figure 4.4 The fluorescence spectral changes (a) and Benesi-Hidebrand plots (b) of **Cum_B** in the presence of different fructose concentration in 10 % DMSO with 0.1 M phosphate buffer at pH 7.4

The detection limit of sensor **cum_B** with fructose was determined by fluorescence spectrophotometry. The sensor **cum_B** was prepared in 5% DMSO with 0.1 M phosphate buffer at pH 7.4 and fluorescence intensity was recorded at 480 nm for 10 times as collected in table 4.1. The detection limit of sensor **Cum_B** toward

fructose calculated by 3SD/slope was found to be 2.83×10^{-3} M in the linear range of 300-1600 μM as showed in fig 4.5.

Table 4.2 Fluorescence intensity of sensor **Cum_B** at 480 nm for 10 times repettion and its standard deviation

Point	Intensity
1	255.7691
2	254.4557
3	255.7449
4	256.9987
5	253.6983
6	254.2599
7	252.6839
8	252.8053
9	254.0856
10	253.1355
SD	1.419071
3SD	4.257213

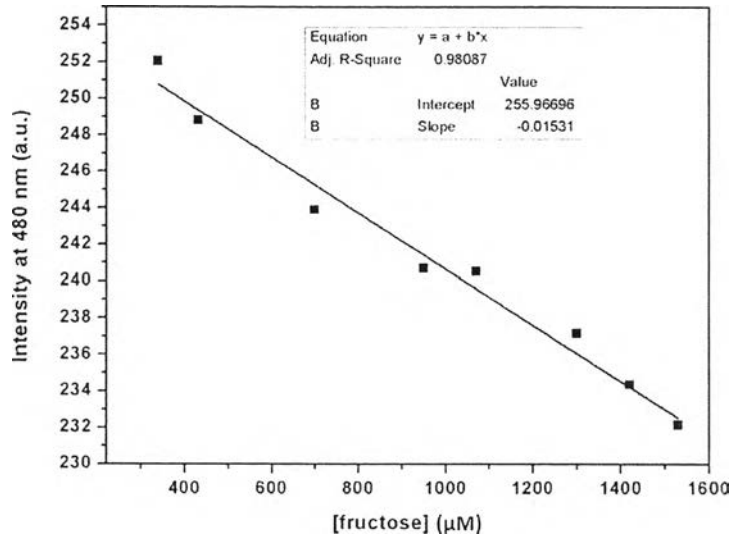

Figure 4.5 Linear plots of fluorescence intensity between **Cum_B** with various concentrations of fructose in 5 % DMSO with 0.1 M phosphate buffer at pH 7.4

Considerably, **Cum_B** showed a high selectivity toward fructose over other saccharides. To verify the binding mode of **Cum_B** and fructose, the Job's plot analysis of sensor **Cum_B** and fructose was performed in Fig 4.6. The maximum point at 0.5 mole fraction suggests a 1:1 binding mode.

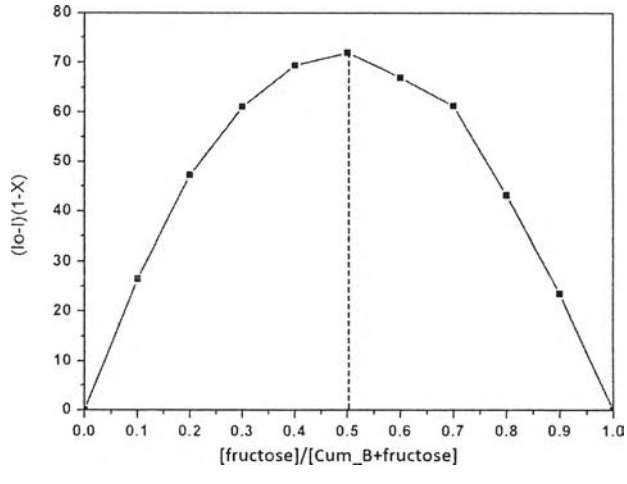

Figure 4.6 Job's plot of the complexation between **Cum_B** (10^{-5} M) and fructose (10^{-5} M) in 0.1 M aqueous phosphate buffer pH 7.4

According to the information results, the sensor **Cum_B** exhibited sensitivity and selectivity with fructose under photo-induced electron transfer process. However, the detection limit and binding constant of **Cum_B** and fructose is still poor. Therefore, we have designed and synthesized a new fluorophore with a new concept of detection to develop the detection limit and binding properties.

4.4 The complexation study of new sensor NBD with saccharide in aqueous solution

4.4.1 Synthesis of NBD

Naphthalimide was selected as the fluorophore owing to excellent photophysical properties [95]. 3-aminophenylboronic acid acts as binding unit and dopamine functions as a linker between naphthalimide and boronic acid. The synthesis pathway of sensors **NBD** was illustrated in Scheme 4.3.

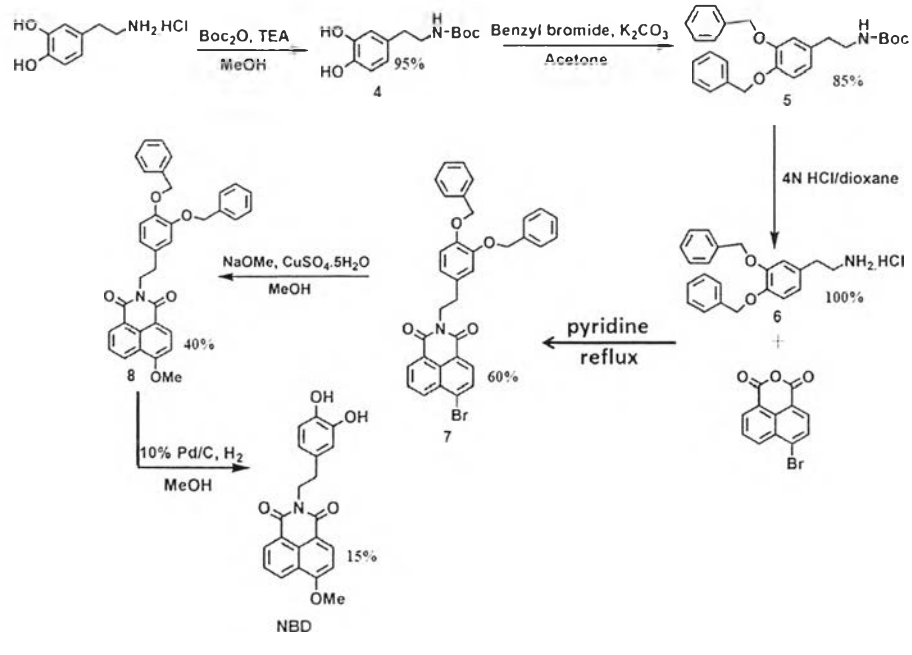

Scheme 4.3 Synthesis pathway of sensor **NBD**

The synthetic pathway started from the protection of the amino group of dopamine. The compound **4** was purified by extraction with dichloromethane to afford a white solid **4** in 95% yield. The ^{1}H-NMR spectrum showed the characteristic peaks of methyl proton of the protecting group at 1.43 ppm.

Compound **5** was prepared by protecting the hydroxyl groups of compound **4** with benzyl bromide to give a white solid in 85% yield. The ^{1}H-NMR spectrum displayed the multiplet peaks of aromatic photons of benzyl group at 7.44-7.28 ppm, doublet peake of ArCH_2 at 5.07 and 5.05 ppm, the quartet peaks of NCH_2CH_2Ar at 3.06–3.07 ppm and triplet peaks of ArCH_2CH_2Nat 2.58–2.55 ppm and the disappearance of hydroxyl signals of dopamine. MALDI-TOF mass spectrum confirmed the structure of compound **5** with the intense peak at 455.50 m/z corresponding to $[M+4H+H_2O]^+$.

Compound **6** was synthesized by deprotecting the amino group of compound **5** with hydrochloric acid/dioxane for 30 minutes. The white solid was obtained without the purification in 100% yield. Then, compound **7** was synthesized by nucleophilic addition between 4-bromo-1,8-naphthalic and compound **6**. The product was purified by column chromatography using a gradient of ethyl acetate in dichloromethane (5:95) as eluent, to obtain pale yellow solid 60% yield. The ^{1}H-NMR data of compound **7** showed the range of aromatic protons of naphthalic moiety at 8.54-7.95 ppm. Interestingly, the singlet proton of ArCH_2 shift to upfield at 5.04 and 4.98 ppm while the quartet peak of NCH_2CH_2Ar and the aliphatic ethylene protons (NCH_2CH_2Ar) showed downfield shift at 4.19-4.16 ppm and 2.83-2.79 ppm, respectively, because of the electron withdrawing group of carbonyl unit. MALDI-TOF

mass spectrum confirmed the structure of compound **7** with the intense peak at 543.20 m/z.

Nucleophilic substitution of compound **8** was synthesized by the reaction between compound **7** and sodium methoxide in methanol. The product was obtained the pale green solid in 40% yield. The ^{1}H-NMR data of compound **8** displayed the characteristic peaks of singlet of the methyl protons (OCH_3) at 4.10 ppm. MALDI-TOF mass spectrum confirmed the structure of compound **8** with the intense peak at 543.42 m/z.

Finally, the **NBD** was prepared by deprotecting the hydroxyl group of compound **8** with 10% Pd/C in methanol for 24 hours under hydrogen atmospheres. The final product is a pale green solid in 15% yield. The ^{1}H-NMR data of **NBD** displayed the quartet and multiplet of NCH_2CH_2Ar at 4.15-4.14 ppm and 2.71-2.67 ppm respectively. Interestingly, the appearance of singlet assignment of hydroxyl group at 8.82 and 8.67 ppm and the disappearance of aromatic protons of benzyl moieties at 7.40–7.30 ppm were observed.

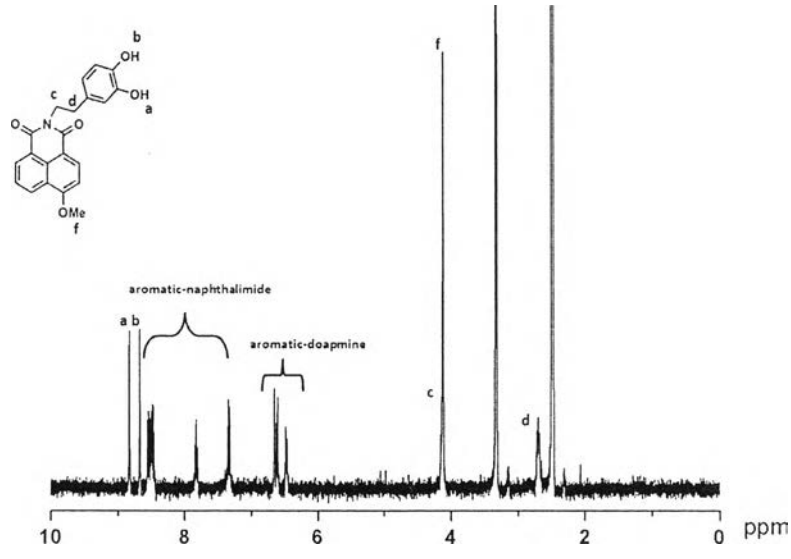

Figure 4.7 The ^{1}H-NMR spectrum of **NBD** in DMSO-d_6 (400MHz).

4.5 The properties of gold nanoparticles

A gold nanoparticle used in this research was prepared by citrate as stabilizer and sodium borohydride as reducing agent. Generally, hydrogen tetrachloroaurate and sodium citrate were stirring to reduce Au^{3+} to Au^{0}. The complete reduction was monitored by color change from pale yellow to red color. After purified by centrifugation at 10000 rpm to remove sodium borohydride, the gold nanoparticles with negative charge of citrate as stabilizer were obtained. Gold nanoparticles were characterized by UV-visible spectroscopy. The characteristic peak of absorption band appeared at 520 nm referred to the average particle size at 14.9 nm [101] as displayed in figure 4.8.

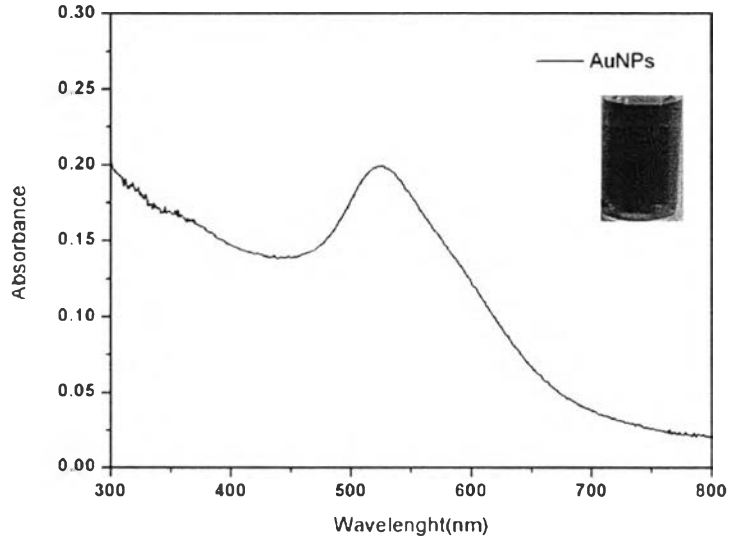

Figure 4.8 UV-Visible spectrum of gold nanoparticles using citrate as stabilizer in H_2O.

4.6 Complexation studies

4.6.1 Complexation studies of sensor NBDB with saccharides

We designed the fluorescence sensor containing **NBD** as a fluorophore and 3-aminoboronic acid as a binding unit to covalently bond with diol moieties of saccharides via reversible ester formation. The absorption band and emission band of **NBD** in 10% DMSO with 0.1 M phosphate buffer at pH 7.4 centered at 375 nm and 460 nm, respectively. The adduct (**NBDB**) of 3-aminoboronic acid with **NBD** performed the slight enhancement of fluorescence intensity as shown in Fig 4.9.

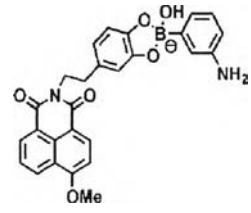

NBDB

Scheme 4.4 Structure of designed receptor based on napthalimide and phenylboronic acid.

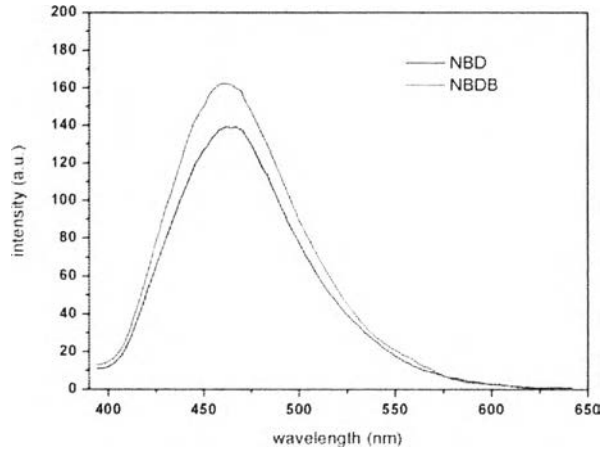

Figure 4.9 Emission spectra of **NBD** and **NBDB** in 10 % DMSO with 0.1 M phosphate buffer at pH 7.4.

When various saccharides are added to the **NBDB** complex, a slight increase of fluorescence intensity was observed as displayed in Fig 4.10. It suggestes that the complex between saccharide and receptor was formed. The fluorescence response of **NBDB** showed the insignificant changes in the presence of various saccharides possibly caused by electron-donating substituent groups located on the naphthalene ring inducing the reduction of the energy of gap between HOMO and LUMO [95]. From the fluorescence changes, this **NBDB** complex bound with saccharides with non-specific binding.

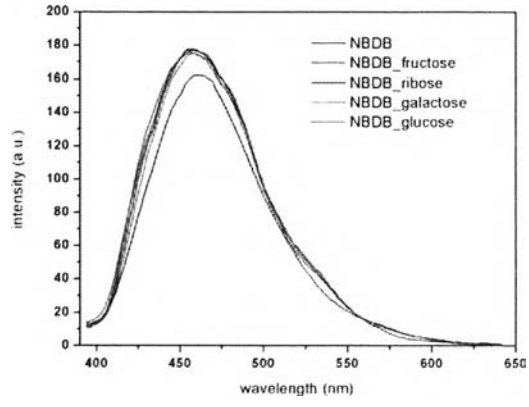

Figure 4.10 Fluorescence spectral changes of **NBDB** with various saccharides in 10 % DMSO with 0.1 M phosphate buffer at pH 7.4.

4.6.2 Complexation studies of sensor NBDB capped gold nanoparticles with saccharides

Due to a small change of fluorescence and non-specific binding of **NBDB** with various saccharides, we have developed the fluorescence responses of detection by using gold nanoparticles to amplify the fluorescence responses. In our concept, we employed gold nanoparticles to quench the fluorescence of **NBDB** which was attracted on AuNPs [102]. Upon addition of guest, we expected that the selective guest can bind with boronic acid based on AuNPs and subsequently cleave fluorophore from AuNPs inducing the fluorescence-on approach. The conceptual illustration was shown in Scheme 4.5.

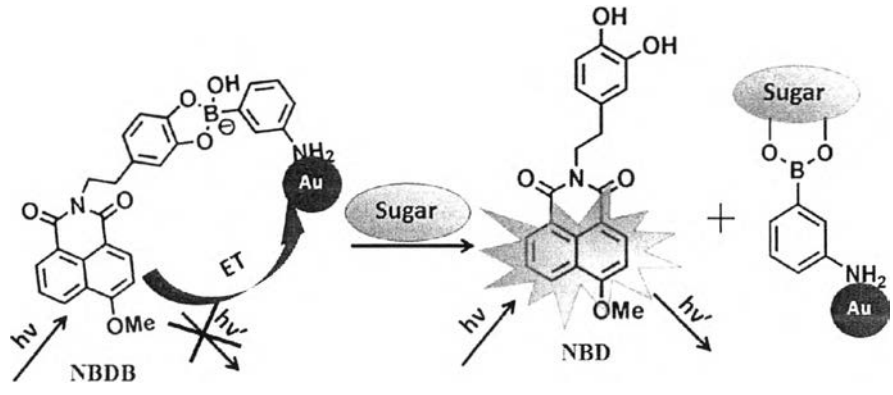

Scheme 4.5 The conceptually proposed structure and saccharides sensing by gold nanoparticles via energy transfer (ET).

4.6.2.1 Modification of gold nanoparticles with NBDB in aqueous solution

Herein, we describe the preparation of fabrication of **NBDB** on the surface of AuNPs. Functionalized gold nanoparticles with **NBDB** were prepared by phase-transfer process. **NBDB** in dimethyl sulfoxide and gold nanoparticles in aqueous buffer solution were mixed together and vigorously stirred for 30 min. The modified gold nanoparticles with **NBDB** exhibited a shift of the surface plasmon absorption band of modified gold nanoparticles from 520 nm to 523-525 nm (Figure 4.11). The absorption changes are a result of the alteration of electronic properties of **NBDB** receptor upon binding with gold nanoparticles via the hydrophobic interaction between the amine based boronic acid and gold nanoparticles. To optimize the concentration of AuNPs in efficient quencher, the fluorescence responses of **NBDB** in the presence of various concentration of AuNPs were investigated in figure 4.12. The fluorescence spectrum showed a large quench upon adding AuNPs at concentration of 14 μM. Conversely, a high concentration of AuNPs causes a slight fluorescence

quenching due to the aggregation of gold nanoparticles of interparticle surface plasmon coupling.

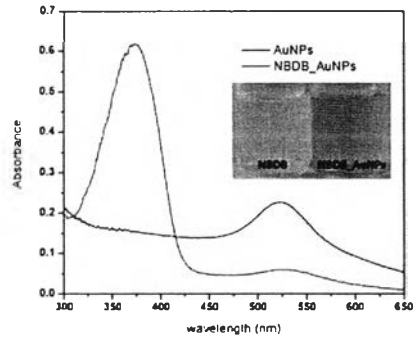

Figure 4.11 UV-visible spectra of modified gold nanoparticles with **NBDB** in 10 % DMSO with 0.1 M phosphate buffer at pH 7.4

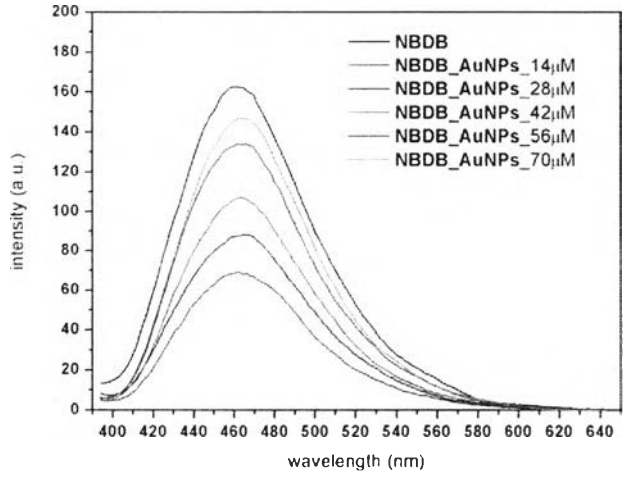

Figure 4.12 Fluorescence spectra of **NBDB** with varying the concentration of gold nanoparticles in 10 % DMSO with 0.1 M phosphate buffer at pH 7.4

4.6.2.2 Complexation studies of sensor NBDB modified gold nanoparticles with saccharides (NBDB_AuNPs) in aqueous solution

The complexation abilities of NBDB functionalized gold nanoparticles for detection of saccharides were investigated in 10% DMSO: phosephate buffer pH 7.4 by UV-Vis and fluorescence spectrophotometry. The calibration curve of complexation between NBD and 3-aminophenylboronic acid were examined to verify the % loading of NBDB on gold nanoparticles (figure 4.13). The concentration of $1x10^{-6}$ M NBD and $1x10^{-5}$ M 3-aminophenylboronic acid on AuNPs (concentration of AuNPs at 14 μM) give the loading of NBDB on AuNPs at approximately 96-99 % suggesting that sensor NBDB preferentially bound with gold nanoparticles.

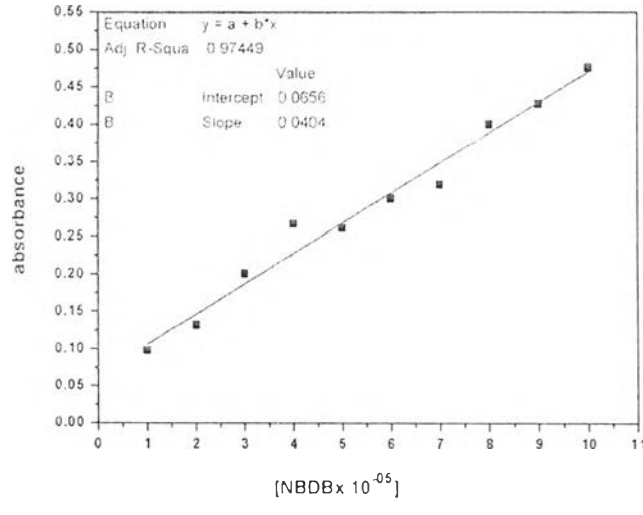

Figure 4.13 Calibration curve of complexation between NBD and 3-aminoboronic acid in 10 % DMSO with 0.1 M phosphate buffer at pH 7.4

Moreover, the sensing ability of NBDB_AuNPs was investigated by the fluorescence technique. The fluorescence spectum of the NBDB_AuNPs in the

presence of fructose demonstrates the significant fluorescence enhancement, whereas other sacchsrides including glucose, galactose and ribose induced a small change of fluorescence intensity of **NBDB_AuNPs** as shown in figure 4.14. Since fructose would cleave **NBD** sensor from **NBDB_AuNPs** and subsequently bind with boronic acid on AuNPs resulting in an inhibition of energy transfer process from fluorophore **NBD** to **AuNPs**. According to Figure 4.14 with the concomitant result of **NBD** with fructose, **NBDB** prefers to bind with fructose over other saccharides. However, **NBDB_AuNPs** shows a larger change of fluorescence intensity than free **NBDB** without AuNPs.

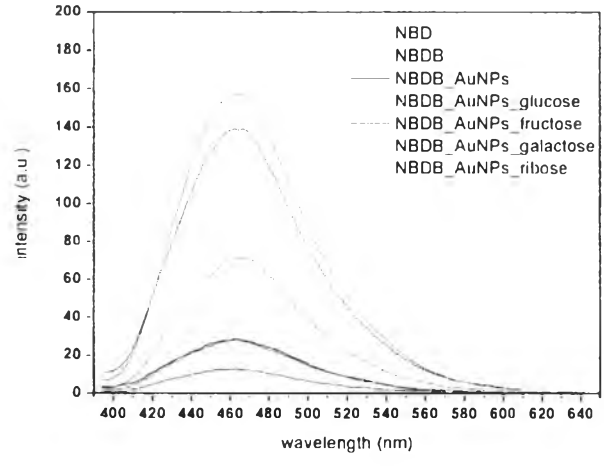

Figure 4.14 Fluorescence spectrum of **NBDB** bind gold nanoparticles in the presence of different saccharides in 10 % DMSO with 0.1 M phosphate buffer at pH 7.4

Since **NBDB_AuNPs** shows a change of fluorescence intensity in the presence of fructose, the binding constant of **NBDB_AuNPs** and fructose was carried out by fluorescence titration as shown in Fig 4.15. Fluorescence titration of fructose into the

aqueous solution of 10^{-4} M **NBD**, aminophenylboronic acid (10^{-5}M) and 14 μM gold nanoparticles upon increment of fructose concentration caused the enhacenment of fluorescence intensity. The **NBDB_AuNPs** system also allows the quantitative determination of binding constants of **NBDB_AuNPs** with fructose by the Benesi-Hidebrand method (fig 4.16).

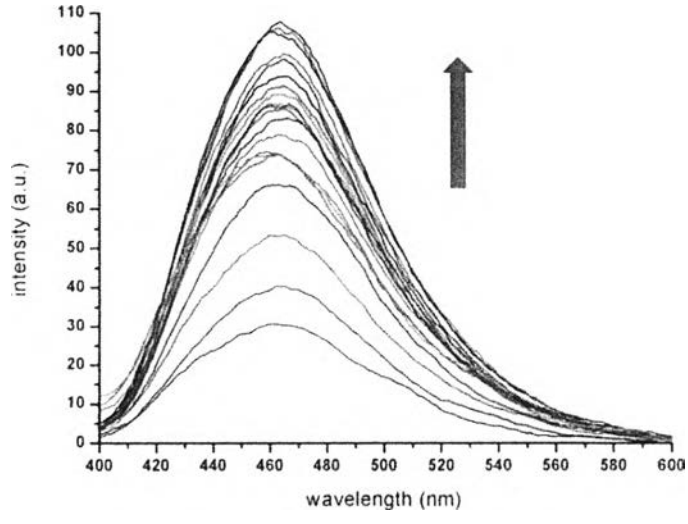

Figure 4.15 The fluorescence spectral changes of **NBDB_AuNPs** in the presence of different fructose concentration (0-4 mM) in 10 % DMSO with 0.1 M phosphate buffer at pH 7.4

According to Benesi-Hidebrand method, the log K_s value of complex **NBDB_AuNPs** with fructose was found to be 4.35.

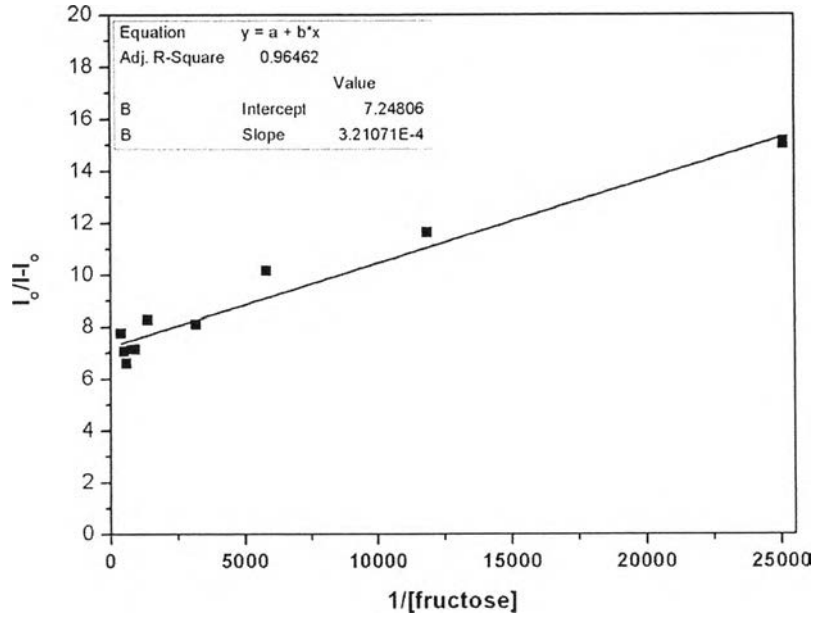

Figure 4.16 Benesi-Hidebrand plots of **NBDB_AuNPs** in the presence of different fructose concentration (0-4 mM) in 10 % DMSO with 0.1 M phosphate buffer at pH 7.4

The detection limit of **NBDB_AuNPs** toward fructose was measured by fluorescence technique. The sensor **NBDB_AuNPs** was prepared in 10 % DMSO with 0.1 M phosphate buffer at pH 7.4 and fluorescence intensities were recorded at 375 nm for 10 times and the results were listed in Table 4.3.

Table 4.3 Fluorescence intensity data of free sensor **NBDB_AuNPs** at 375 nm for 10 times repeatition and its standard deviation

Point	Intensity
1	98.55464
2	98.39867
3	100.3933
4	98.11013
5	98.7499
6	95.5638
7	99.34479
8	97.48654
9	96.83884
10	96.59962
SD	1.417562
3SD	4.252686

The detection limit of **NBDB_AuNPs** toward fructose in 10 % DMSO with 0.1 M phosphate buffer at pH 7.4 calculated on the basis of 3SD/slope was $1.5x10^{-3}$ M.

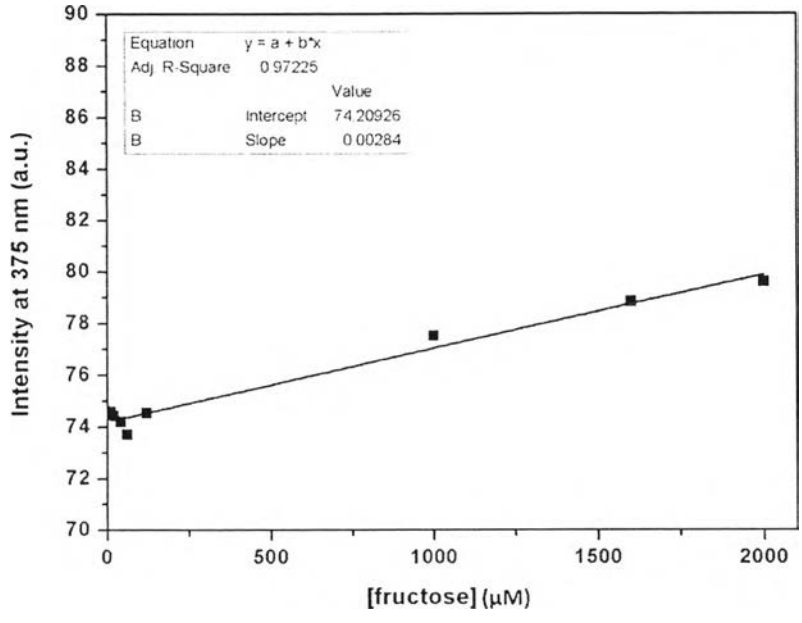

Figure 4.17 Linear plots of fluorescence intensity of **NBDB_AuNPs** versus concentration of fructose in 10 % DMSO with 0.1 M phosphate buffer at pH 7.4

Compared to the sensing affinity of **Cum_B**, **NBDB_AuNPs** offers more excellently sensing ability toward fructose in terms of the binding constant and the detection limit.